AGU PUBLICATIONS

Journal of Advances in Modeling Earth Systems

RESEARCH ARTICLE

10.1002/2013MS000294

Key Points:
- Changes in the ventilation index are calculated for the RCP8.5 scenario
- There is a general tendency for the ventilation to increase in the tropics
- Tropical cyclone activity changes correlate well with ventilation changes

Correspondence to:
B. Tang,
btang@albany.edu

Citation:
Tang, B., and S. J. Camargo (2014), Environmental control of tropical cyclones in CMIP5: A ventilation perspective, *J. Adv. Model. Earth Syst.*, *6*, 115–128, doi:10.1002/2013MS000294.

Received 8 DEC 2013
Accepted 10 JAN 2014
Accepted article online 16 JAN 2014
Published online 24 FEB 2014

Environmental control of tropical cyclones in CMIP5: A ventilation perspective

Brian Tang[1] and Suzana J. Camargo[2]

[1]Department of Atmospheric and Environmental Sciences, University at Albany – State University of New York, Albany, New York, USA, [2]Lamont-Doherty Earth Observatory, Columbia University, Palisades, New York, USA

Abstract The ventilation index serves as a theoretically based metric to assess possible changes in the statistics of tropical cyclones to combined changes in vertical wind shear, midlevel entropy deficit, and potential intensity in climate models. Model output from eight Coupled Model Intercomparison Project 5 models is used to calculate the ventilation index. The ventilation index and its relationship to tropical cyclone activity between two 20 year periods are compared: the historical experiment from 1981 to 2000 and the RCP8.5 experiment from 2081 to 2100. The general tendency is for an increase in the seasonal ventilation index in the majority of the tropical cyclone basins, with exception of the North Indian basin. All the models project an increase in the midlevel entropy deficit in the tropics, although the effects of this increase on the ventilation index itself are tempered by a compensating increase in the potential intensity and a decrease in the vertical wind shear in most tropical cyclone basins. The nonlinear combination of the terms in the ventilation index results in large regional and intermodel variability. Basin changes in the ventilation index are well correlated with changes in the frequency of tropical cyclone formation and rapid intensification in the climate models. However, there is large uncertainty in the projections of the ventilation index and the corresponding effects on changes in the statistics of tropical cyclone activity.

1. Introduction

There remains large uncertainty in how global and regional tropical cyclone (TC) activity will respond to large-scale changes in the climate system due to anthropogenic forcing. Two main approaches have been used to study this problem: examining TC-like vortices in global climate models (GCMs) [*Bengtsson et al.*, 1996; *Oouchi et al.*, 2006; *Yoshimura et al.*, 2006; *Bengtsson et al.*, 2007; *Sugi et al.*, 2009; *Zhao et al.*, 2009; *Murakami et al.*, 2012] and downscaling GCM fields using a higher resolution model or statistical methods [*Knutson and Tuleya*, 2004; *Emanuel et al.*, 2008; *Knutson et al.*, 2008; *Garner et al.*, 2009; *Bender et al.*, 2010; *Zhao and Held*, 2010; *Hill and Lackmann*, 2011; *Villarini and Vecchi*, 2012; *Emanuel*, 2013; *Knutson et al.*, 2013; *Villarini and Vecchi*, 2013]. *Knutson et al.* [2010] arrived at a consensus estimate of a global decrease in TC frequency of 6–34% and an increase in intensity of 2–11% by 2100 for the A1B emissions scenario from the third iteration of the Coupled Model Intercomparison Project (CMIP). However, there is large variability between different ocean basins and GCMs. Additionally, one downscaling study using the latest iteration of GCMs in CMIP5 is well outside the range of the prior consensus, casting larger uncertainty on projections of changes in global TC activity [*Emanuel*, 2013].

The shifts in TC frequency and intensity noted in GCMs are driven in part by changes in the distributions of environmental variables that are known to influence genesis and intensity in current climate. For example, *Vecchi and Soden* [2007a] and *Garner et al.* [2009] noted that a consensus of GCMs project an increase in vertical wind shear from the Caribbean to the central North Atlantic. They hypothesize that such a pattern would result in more hostile conditions for TCs in this region. However, most GCMs also project a small increase in potential intensity over most of the tropics that would make thermodynamic conditions more favorable. Hence, there are competing signals, and it is unclear which effect dominates.

One way to assess the effect of different environmental variables is to regress them on to the spatial and temporal distribution of tropical cyclogenesis events or accumulated statistics of TC intensity [*Emanuel*, 2007, 2010; *McGauley and Nolan*, 2011; *Tippett et al.*, 2011]. For example, *Emanuel* [2010] formulated a genesis potential index with four environmental variables: potential intensity, low-level absolute vorticity, deep-layer vertical wind shear, and nondimensional entropy deficit. *Tippett et al.* [2011] formulated a genesis potential index

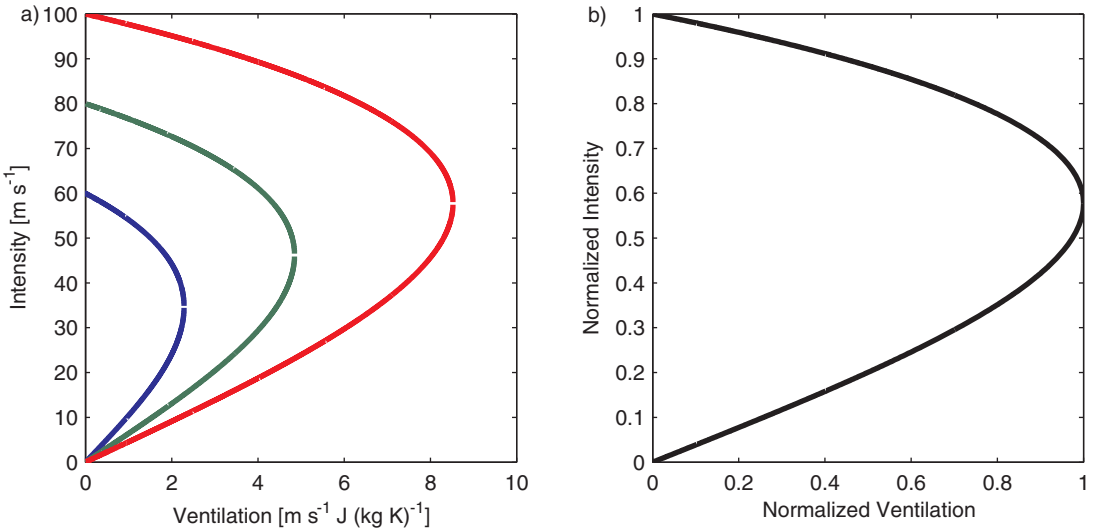

Figure 1. (a) Equilibrium intensities for three different potential intensities as a function of the ventilation. The upper part of each curve is the stable equilibrium intensity, and the lower part of each curve is the unstable equilibrium intensity. (b) The normalized equilibrium intensity as a function of the normalized ventilation after nondimensionalizing Figure 1a.

using the relative sea surface temperature (SST), defined as the local SST minus the tropical mean SST, and midlevel relative humidity in lieu of the potential intensity and nondimensional entropy deficit, respectively.

The difficulty in constructing TC indices empirically is that there are many combinations of variables and statistical methods that one can use to perform this exercise. Additionally, it is unknown how robust these indices are with climate change, since they are trained on the current climatology of TCs. Therefore, it would be advantageous to construct these indices based on variables that are theoretically relevant to TC genesis and intensity, independent of ocean basin, and invariant with changing climate. One variable that is a candidate for these requirements is the ventilation index.

2. Ventilation Index

Ventilation is defined as the flux of low-entropy air into a tropical disturbance or TC. With respect to genesis, ventilation disrupts the formation of a deep, moist column that is hypothesized to be imperative for the spin up of the vortex [*Emanuel*, 1989; *Bister and Emanuel*, 1997; *Nolan*, 2007; *Rappin et al*., 2010]. After genesis, vertical wind shear acts to decrease the efficiency of the TC heat engine by increasing the entrainment of low-entropy parcels into the inner-core convection [*Simpson and Riehl*, 1958; *Cram et al*., 2007; *Marín et al*., 2009] and flushing the boundary layer with downdrafts [*Powell*, 1990; *Riemer et al*., 2010; *Riemer and Montgomery*, 2011]. These processes counteract the generation of available potential energy by surface fluxes and weaken the TC [*Tang and Emanuel*, 2012a].

Tang and Emanuel [2010] developed an idealized framework to study the effects of ventilation on TCs. The fundamental result is an analytical system describing the intensity of ventilated TCs, as shown in Figure 1a. Each curve represents the equilibrium intensity of a TC as a function of the dimensional ventilation (The ventilation is the integrated eddy flux of entropy perpendicular to the angular momentum surface bounding the outer eyewall scaled by the downdraft area [*Tang and Emanuel*, 2010].) for a given potential intensity, given by where the upper part of each curve intersects the vertical axis. Different curves represent spatially or temporally varying background environments, such as caused by climate change. By normalizing the equilibrium intensity by the potential intensity and the ventilation by the ventilation threshold, given by the ventilation value at the vertex of each curve, a nondimensional system is obtained in which all the curves collapse to a single curve, as shown in Figure 1b. A strengthening or steady TC can only exist if the normalized ventilation is less than or equal to one, whereas the equivalent bound of the dimensional ventilation changes with the background environment. The normalization is highly advantageous because the normalized ventilation may then be used to compare ventilation effects on TCs across varying thermodynamic states caused by climate change in a consistent manner.

Table 1. CMIP5 Modeling Institutions and GCM Acronyms [*Taylor et al.*, 2012]

Institution(s)	Model
Centre National de Recherches Meteorologiques, Centre Europeen de Recherche et Formation Avancees en Calcul Scientifique	CNRM-CM5
Commonwealth Scientific and Industrial Research Organization, Queensland Climate Change Centre of Excellence	CSIRO-Mk3.6.0
Geophysical Fluid Dynamics Laboratory	GFDL-ESM2M
Atmosphere and Ocean Research Institute, National Institute for Environmental Studies, Japan Agency for Marine-Earth Science and Technology	MIROC5
Met Office Hadley Center	MOHC-HadGEM2CC
Max Planck Institute for Meteorology	MPI-ESMMR
Meteorological Research Institute	MRI-CGCM3
National Center for Atmospheric Research	NCAR-CCSM4

The functional form of the normalized ventilation is complicated, but *Tang and Emanuel* [2012b] showed that the normalized ventilation scales with (bulk) environmental parameters, yielding a much easier ventilation metric to calculate with relatively coarse CMIP5 data that retains the key advantage of invariance with climate. This metric is called the ventilation index, Λ:

$$\Lambda = \frac{u_{\text{shear}}\,\chi_m}{u_{\text{PI}}}, \tag{1}$$

where u_{shear} is the 850–250 hPa bulk vertical wind shear, χ_m is the nondimensional entropy deficit, and u_{PI} is the potential intensity. The nondimensional entropy deficit is defined as

$$\chi_m = \frac{s_m^* - s_m}{s_{SST}^* - s_b}, \tag{2}$$

where s_m, s_{SST}, and s_b are the moist entropies at 700 hPa, the sea surface, and of the boundary layer, respectively. The asterisk denotes the saturation moist entropy. Details on how to calculate both equations (1) and (2) are given in *Tang and Emanuel* [2012b]. The levels chosen here are based on data availability in the CMIP5 archive.

The ventilation index can be thought as a ratio of "antifuel" to "fuel" terms. Vertical wind shear allows low-entropy air to intrude into the high-entropy reservoir of the inner core. The intrusion partially negates the energy supplied by surface fluxes, destroying available potential energy and frustrating its conversion to mechanical energy. However, greater surface fluxes (potential intensity) can buffer against the debilitating effects of ventilation by counteracting the intrusion of low-entropy air. With regards to climate change, how the "antifuel" terms change relative to the available "fuel" is the key question.

3. Ventilation Changes in GCMs

The ventilation index is calculated using daily data from the CMIP5 archive [*Taylor et al.*, 2012]. Only a subset of the CMIP5 models, listed in Table 1, are examined, primarily based on availability of daily data required for calculating the ventilation index. For each model, the ventilation index is calculated over two 20 year periods: 1981–2000 in the historical experiment and 2081–2100 in the RCP8.5 experiment. Statistics of the ventilation index are then compared between these two periods during the peak 4 month season of each hemisphere's TC season to assess changes in the ventilation and infer potential effects on TCs. The Northern Hemisphere peak TC season is defined to be July through October, and the Southern Hemisphere season is defined to be December through March. Hereafter, all analyses are calculated and compared over the same seasonal time frames.

The RCP8.5 experiment simulates a high-end emissions scenario in which anthropogenic emissions and policy decisions lead to a radiative forcing of 8.5 W m^{-2} by 2100. The resulting forcing induces changes in the general circulation and thermodynamic environment in the tropics that affect the variables on the right-hand side of equation (1), which then combine nonlinearly to affect the ventilation index.

Figure 2 shows the percent change in the median ventilation index from the historical to RCP8.5 experiments. The median is chosen over the mean to avoid the tail of the distribution having unrepresentative

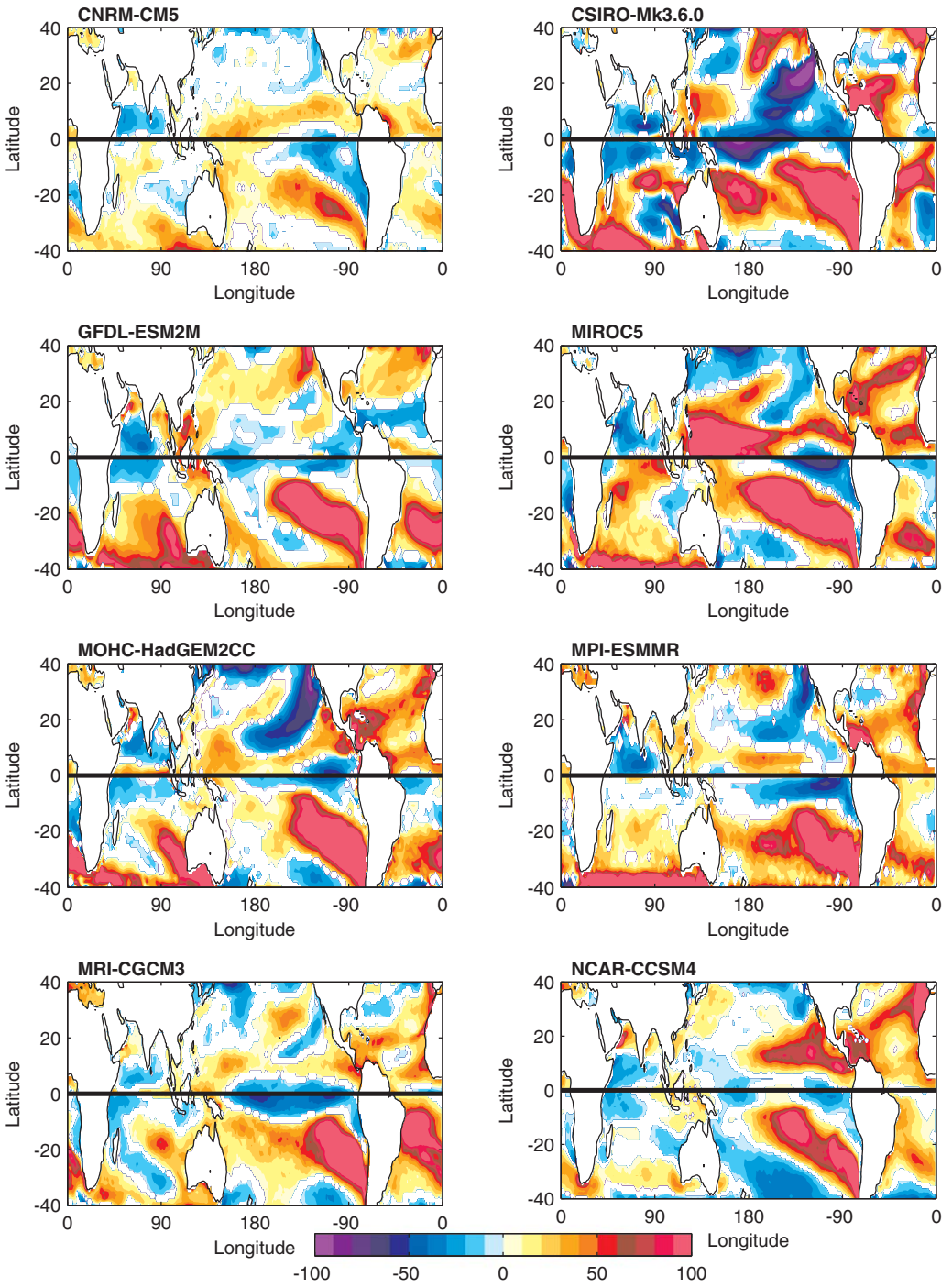

Figure 2. Percent change in the median ventilation index for eight GCMs from 1981–2000 to 2081–2100 for the RCP8.5 scenario.

effects on the statistics. Points where the median is not significantly different between the two experiments at the 95% level using the Kruskal-Wallis test are masked out.

Changes in the ventilation index vary by region and by model. For instance in the North Atlantic, the CSIRO-Mk3.6.0, MIROC5, MOHC-HadGEM2CC, MPI-ESMMR, MRI-CGCM3, and the NCAR-CCSM4 show increases in the median ventilation index, particularly in the Caribbean where the change is in excess of 50%. The CNRM-CM5 shows very little change in the North Atlantic. In fact, the CNRM-CM5 shows the least change in the ventilation index over much of the tropics. On the other hand, the GFDL-ESM2M shows small decreases

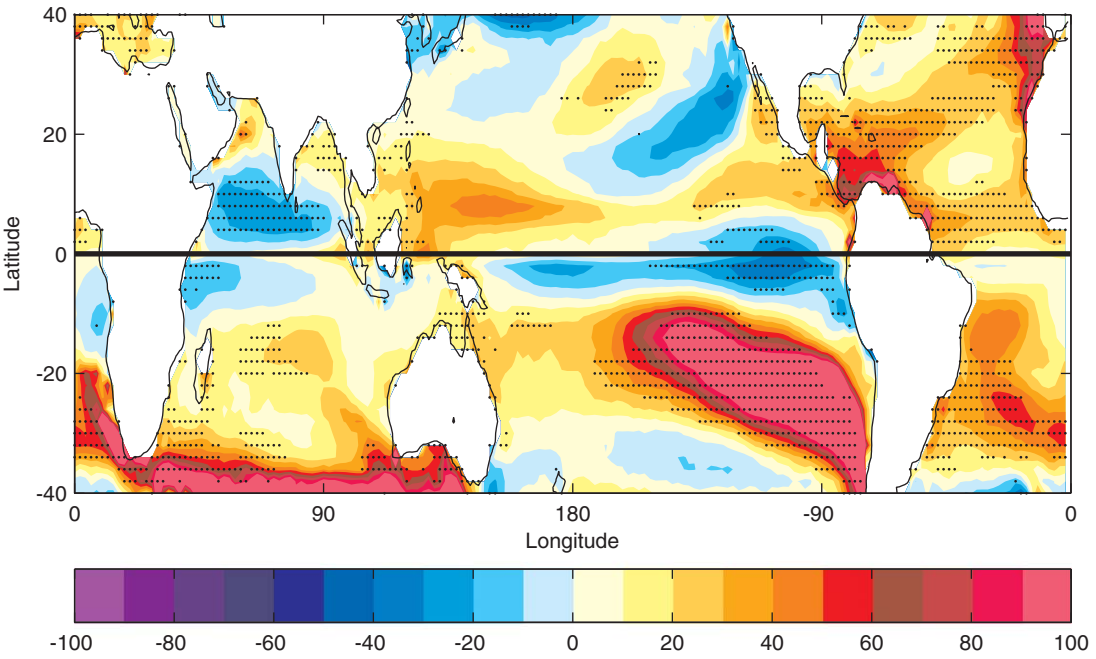

Figure 3. The eight-GCM ensemble average of the change in the median ventilation index from 1981–2000 to 2081–2100 for the RCP8.5 scenario. Stippled areas denote where the ensemble average change exceeds the ensemble standard deviation.

of 10–40% in the Caribbean and the main development region of the Atlantic. Another climatologically active region for TCs is the area from the Philippines to the dateline. Here, the MIROC5 shows increases in the median ventilation index exceeding 100%. The CSIRO-Mk3.6.0, MOHC-HadGEM2CC, and MRI-GCM3 show smaller increases, generally less than 60%. The remainder of the models project mixed, but small, increases and decreases. The general theme is there is large regional and intermodel variability in the RCP8.5 projections of changes in the median ventilation index. The RCP4.5 projections have similar spatial patterns, but tend to be lower in magnitude (not shown).

Figure 3 shows the multimodel ensemble average of the change in the median ventilation index after each model is interpolated to a $2^\circ \times 2^\circ$ grid. Stippled areas mark where the change exceeds the multimodel standard deviation, similar to what is done in the Intergovernmental Panel on Climate Change reports, to denote where the changes in the median of the ventilation index have a higher signal to noise ratio. While one must keep in mind the small sample size of the models examined in this study, there does appear to be a signal for a 20–60% increase in the median ventilation index around Mexico, the Caribbean, central North Atlantic, and South Atlantic. There are smaller increases around 10–30% in pockets around southeast Asia, off the north coast of Australia, and the central South Indian. The largest increases in the median ventilation index are in the southeast Pacific away from the equator. However, this area already has a dearth of TC activity and conditions are only projected to get more hostile for TCs from a ventilation perspective. On the other hand, the model consensus has a decrease in the median ventilation index of 10–30% in the North Indian, away from the Arabian Sea and Bay of Bengal, and the equatorial East Pacific.

Basin-by-basin changes in the median ventilation index are shown in Table 2. Figure 4 shows the basins over which the quantities in Table 2 are calculated, minus any land areas. Additionally, basin changes in the median vertical wind shear, nondimensional entropy deficit, and potential intensity are calculated in order to infer what combination of variables drives the projected changes in the median ventilation index. All but the GFDL-ESM2M model show a significant increase in the median ventilation index in the North Atlantic, which is largely driven by increases in the nondimensional entropy deficit. This increase is somewhat ameliorated by increases in the median potential intensity by 3–6%. Changes in the median vertical wind shear are not as robust, albeit those models that are significant show slight decreases in the vertical wind shear, which also act to compensate a small amount for the increase in the nondimensional entropy deficit.

Table 2. Basin-by-Basin Percent Changes[a] in the Median Vertical Wind Shear, Nondimensional Entropy Deficit, Potential Intensity, and Ventilation Index From 1981–2000 to 2081–2100 for the RCP8.5 Scenario

Basin	Variable	CNRM	CSIRO	GFDL	MIROC	HadGEM	MPI	MRI	NCAR
N Atlantic	u_{shear}	**−3**	0	**−7**	−4	**−2**	−1	0	−1
	χ_m	**19**	**37**	**16**	**49**	**49**	**40**	**23**	**40**
	u_{PI}	**6**	**6**	**5**	**5**	**6**	**4**	**4**	**3**
	Λ	**8**	**28**	0	**36**	**38**	**29**	**18**	**36**
NE Pacific	u_{shear}	−2	**−4**	**−8**	**−9**	2	**−9**	**4**	**12**
	χ_m	**19**	1	**15**	**52**	**28**	**20**	**10**	**38**
	u_{PI}	**3**	**14**	**2**	**7**	**7**	**6**	**5**	**2**
	Λ	**14**	**−21**	2	**32**	**28**	1	**12**	**55**
NC Pacific	u_{shear}	**−10**	**−14**	**−5**	**−17**	**−22**	**−11**	−3	3
	χ_m	**21**	**13**	**18**	**32**	8	**10**	**16**	**24**
	u_{PI}	**6**	**19**	**3**	**5**	**9**	**8**	**5**	**3**
	Λ	2	**−13**	6	1	**−23**	**−9**	6	**25**
NW Pacific	u_{shear}	**−6**	**−4**	2	**−6**	**−9**	**−4**	−2	−4
	χ_m	**15**	**19**	**10**	**55**	**27**	**13**	**10**	**10**
	u_{PI}	**4**	**5**	0	**6**	**6**	**3**	**5**	**4**
	Λ	5	**11**	12	**34**	**7**	**7**	6	2
N Indian	u_{shear}	−2	**−4**	**−6**	**−12**	**−8**	**−5**	−1	**−5**
	χ_m	**7**	**6**	**6**	**15**	**9**	**10**	**5**	**11**
	u_{PI}	**5**	**8**	0	**7**	**8**	**4**	**5**	**4**
	Λ	−4	**−10**	−4	**−10**	**−12**	−4	−2	−4
S Atlantic	u_{shear}	**−2**	**9**	−2	**−6**	**−10**	−1	**4**	**−5**
	χ_m	**17**	**15**	**43**	**18**	**23**	**24**	**47**	**28**
	u_{PI}	**5**	**11**	−1	**4**	**7**	**4**	**1**	**4**
	Λ	6	**26**	**43**	**16**	8	**16**	**50**	**18**
SE Pacific	u_{shear}	**−4**	**14**	0	1	0	4	**7**	**−4**
	χ_m	**16**	**60**	**43**	**33**	**62**	**39**	**50**	**33**
	u_{PI}	**5**	**−5**	**−2**	0	**−4**	**3**	0	**2**
	Λ	8	**92**	**56**	**42**	**77**	**48**	**62**	**35**
SW Pacific	u_{shear}	2	**13**	**9**	4	1	**3**	**7**	0
	χ_m	**20**	**31**	**19**	**67**	**31**	**27**	**15**	**18**
	u_{PI}	**2**	**4**	−1	1	**3**	**2**	**3**	**2**
	Λ	**19**	**42**	**36**	**75**	**32**	**29**	**20**	**22**
S Indian	u_{shear}	**−3**	−2	−3	**−8**	**−12**	**−4**	**−7**	**−8**
	χ_m	**14**	**31**	**20**	**33**	**31**	**27**	**17**	**16**
	u_{PI}	**5**	**7**	**4**	**7**	**6**	**5**	**6**	**7**
	Λ	4	**26**	**11**	**14**	**8**	**12**	**5**	−1

[a]Bold numbers denote significant changes in the median at the 95% level using the Kruskal-Wallis test.

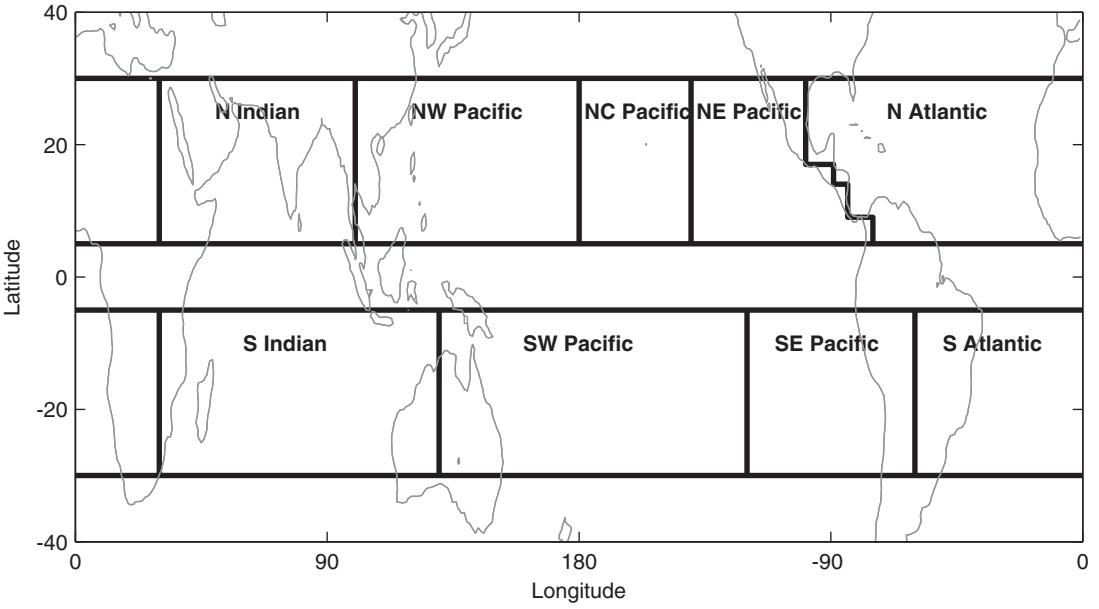

Figure 4. Tropical cyclone basins over which the quantities in Table 2 are calculated.

It is important to emphasize that in the context of the ventilation pathway in TCs, simply looking at changes in vertical wind shear leads to an incomplete view. One needs to look at all three variables in order to gauge the full effect of ventilation. For instance, the majority of the models project a significant decrease in median vertical wind shear in the North-Central and Northwest Pacific basins, which in the context of existing TC-wind shear studies implies more favorable conditions for nonbaroclinic tropical cyclogenesis and intensification of TCs [e.g., *Gray*, 1968; *DeMaria*, 1996]. However, there is also a projected increase in the median nondimensional entropy deficit that increases the thermodynamic difference between any hypothetical TCs and the environment, increasing the potential for ventilation even in the absence of any changes in the vertical wind shear. Additionally, increases in the potential intensity, or an increase in surface fluxes, buffer against some of the effects of the ventilation. Changes in the components can combine to enhance changes in the ventilation index, such as the vertical wind shear and the nondimensional entropy deficit in the NCAR-CCSM4 in the Northeast Pacific, or changes in the components can cancel and result in little change in the ventilation index, such as the CNRM-CM5 and the MIROC5 in the North-Central Pacific.

Despite the variability in the models, there are a few gross patterns in the components of the ventilation index that emerge among the GCMs in Table 2. First, of the basins and models that show significant changes in the vertical wind shear, 78% agree that there will be a decrease in the median vertical wind shear. This decrease is consistent with a weakening of the tropical overturning circulation [*Vecchi and Soden*, 2007b] and a polar migration of the jets [*Barnes and Polvani*, 2013] in the GCMs. The most consistent and largest change is the projected increase in the nondimensional entropy deficit. The reason for this increase can be explained by examining what controls the numerator and denominator of equation (2). As explained by *Emanuel et al*. [2008], the numerator of equation (2) scales as the saturation water vapor mixing ratio, under the assumption of constant relative humidity [*Soden and Held*, 2006], and thus rises exponentially as temperature increases. The denominator increases more slowly because it is tied to the surface enthalpy fluxes at the potential intensity, which is projected to only increase slightly. Despite the relative consistency in the change in sign of the individual variables that comprise the ventilation index, the nonlinear combination of the variables results in much greater scatter in changes in the ventilation index itself.

While the median serves as a convenient metric to gauge changes in the ventilation climatology, examining changes in the complete distribution of the ventilation index is necessary to fully assess potential changes in environments favorable for genesis and intensification. *Tang and Emanuel* [2012b] showed the tropical cyclogenesis preferentially occurs when the ventilation index is anomalously low. Tropical cyclogenesis is defined as the point and time of the first entry in the National Hurricane Center and Joint Typhoon Warning Center best track databases. Using the ERA-Interim reanalysis [*Dee et al*., 2011] to calculate the daily ventilation index one day prior to genesis, 95% of tropical cyclogenesis events from 1981–2000 occur when the ventilation index is less than the 23rd percentile of the daily ventilation index over 5° and 30° N and S.

Tang and Emanuel [2012b] also showed that TC intensification is also more likely to occur when a TC is embedded in anomalously low ventilation indices. However, intensification in the ventilation framework must be viewed in the bivariate space of the ventilation combined with the intensity of the TC (see Figure 1). Since the latter is not well resolved in GCMs, this presents a challenge. However, there is much starker separation in the ventilation indices for rapidly intensifying TCs, where a TC intensifies by at least 15 m s^{-1} over a day, versus the generic population of TCs. Ninety-five percent of rapidly intensifying TCs have ventilation indices less than the 20th percentile of the daily ventilation index over 5° and 30° N and S.

For convenience, we choose the 25th percentile of the daily ventilation index as a soft threshold value that is necessary for both tropical cyclogenesis and rapid intensification. Changes in the lower quartile of the daily ventilation index between the historical and RCP8.5 experiment serve as a proxy for potential changes in tropical cyclogenesis and rapid intensification between these two experiments.

Figure 5 shows the relative frequency change between the historical and RCP8.5 experiments in the daily ventilation index between 5° and 30° N and S. The crosses denote the 25th percentile of the ventilation index distribution in the historical experiment. Recall due to the nondimensional, invariant nature of the ventilation index, this threshold is theoretically not a function of changing climate. The pattern among the various GCMs is consistent. There is a projected decrease in the relative frequency of lower values of the ventilation index and an increase in the relative frequency of higher values of the ventilation index. In other words, there is a shift in the climatological distribution of the ventilation index to the right. This is

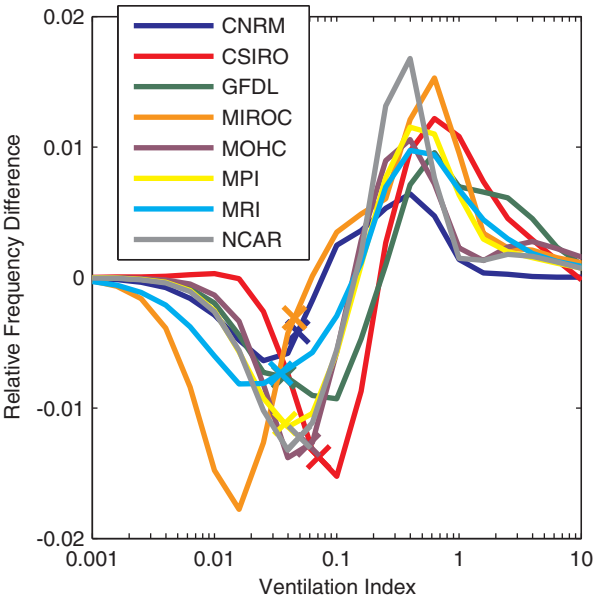

Figure 5. Changes in the climatological distribution of the daily ventilation index between 2081–2100 and 1981–2000 for the RCP8.5 scenario over 5 – 30°. The crosses mark the 25th percentile in the 1981–2000 daily ventilation index for the historical experiment. A logarithmic scale is used for the ventilation index in order to resolve small values.

predominately driven by a shift in the climatological distribution of the nondimensional entropy deficit to the right as well (not shown), consistent with what is seen in changes in the median ventilation index. Hence, the models generally show a decrease in the frequency of days favorable for both genesis and rapid intensification over the tropics.

While there is an overall decrease in the relative frequency of days with favorable ventilation indices in the tropics between the historical and RCP8.5 experiments, there is much more local variability, as shown in Figure 6. While the spatial correlation with changes in the median ventilation index (Figure 2) is very high, especially in the tropics, Figure 6 can be used to project changes in the ventilation favorability, defined as total number of days per season when the daily ventilation index is favorable for tropical cyclogenesis and rapid intensification. For instance, the MIROC5 projects that the ventilation favorability decreases by up to half the season (60 days) east of the Philippines, which would substantially reduce the number of days favorable for tropical cyclogenesis or rapid intensification in that region of the Northwest Pacific. On the other hand, the CSIRO-Mk3.6.0 projects a substantial increase in the ventilation favorability by 40–60 days south of Hawaii. It is evident in each of the models there are nontrivial, local changes to the ventilation favorability that potentially can alter the windows of opportunity for tropical cyclogenesis or rapid intensification by days to weeks. However, there is again a great amount of variability in the ventilation favorability when looking across the models.

Figure 7 shows the multimodel ensemble mean change in ventilation favorability after interpolation to a $2^\circ \times 2^\circ$ grid. Stippled areas denote where the ensemble average exceeds the ensemble standard deviation. In the North Atlantic, there is a general decrease in the ventilation favorability by 6–15 days per season, particularly from the Gulf of Mexico to areas north of the Greater Antilles and in the southern main development region between the Caribbean and west coast of Africa. In the Northeast Pacific and Northwest Pacific near southeast Asia, there is also some indication that the ventilation favorability decreases, but the model spread is generally higher. On the other hand, the ventilation favorability increases in the North Indian by 3–15 days per season in the ensemble mean. In the Southern Hemisphere, the consensus is for a general decrease in the ventilation favorability, particularly between 10 and 20°S in the South Pacific east of the dateline. Here the window is cut by upward of an entire month, which may imply that TC activity will be confined further toward the west. In the South Atlantic, the ventilation favorability decreases by 3–9 days per season.

4. Relationship to TC Activity in GCMs

We now seek to link changes in TC activity in the GCMs to changes in the ventilation index. The 25th percentile of the historical ventilation index distribution again serves as the soft threshold for each GCM, as given by the crosses in Figure 5. The change in the ventilation favorability is now defined as the percent change in the cumulative distribution at the threshold ventilation index value. Changes in the cumulative distribution are due to both spatial and temporal changes in the daily ventilation index between the historical and RCP8.5 experiments. Changes are calculated over each of the basins in Figure 4 between 10 and 20° over the season.

Changes in the ventilation favorability are first compared with changes in TC frequency in the GCMs. The analysis is restricted to four models: CSIRO-Mk3.6.0, GFDL-ESM2M, MIROC5, and MRI-CGCM3, corresponding

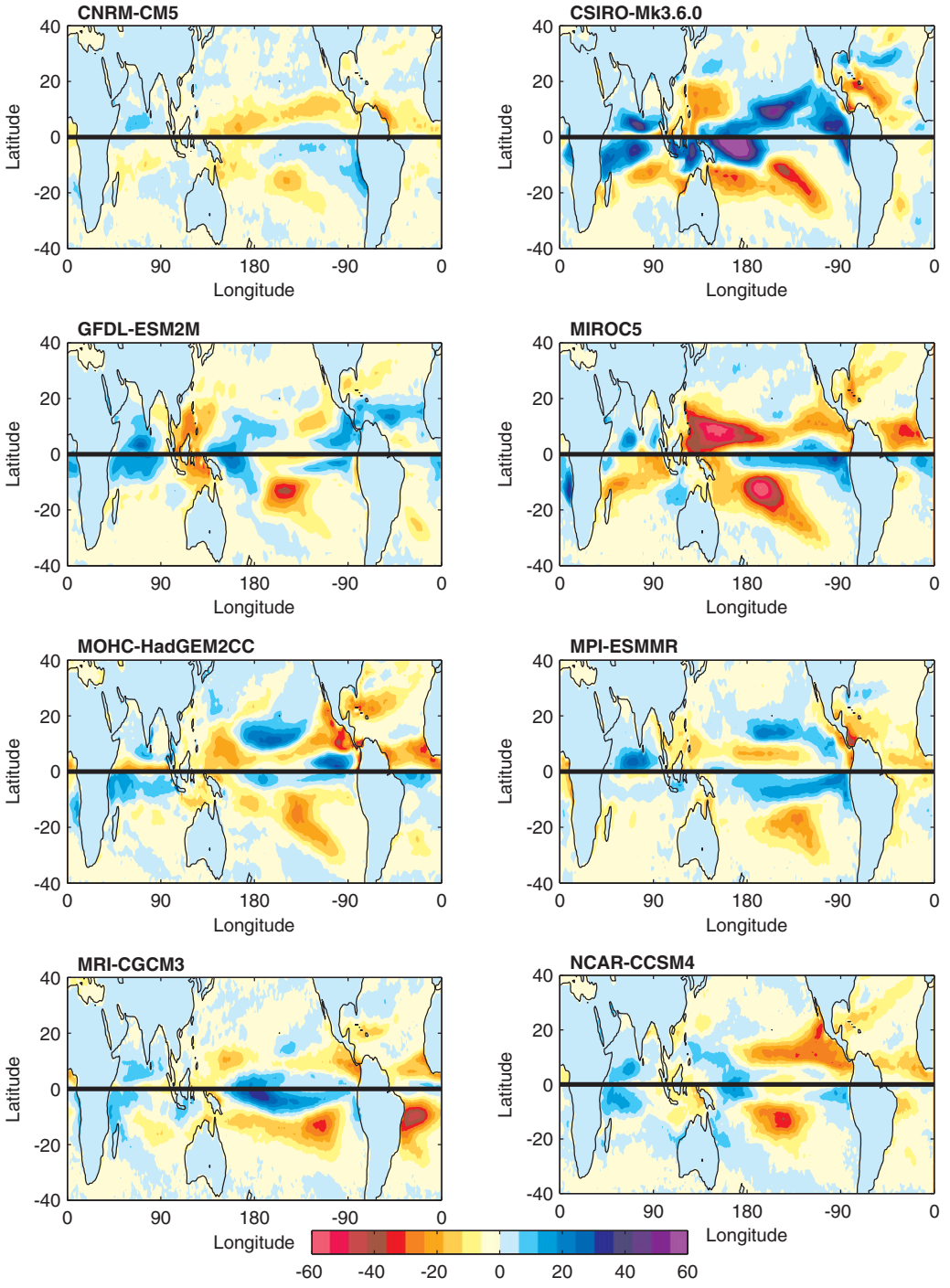

Figure 6. Change in the ventilation favorability, or number of days per season (approximately 120 days) where the daily ventilation index is favorable for tropical cyclogenesis and rapid intensification. Changes are calculated between 2081–2100 and 1981–2000 for the RCP8.5 scenario. Note the reverse color bar for easier comparison with earlier figures.

to overlapping data sets with *Camargo* [2013]. TCs are identified in the GCMs using an algorithm to track vortices having a local maxima in 850 hPa relative vorticity and wind speed, minima in surface pressure, and warm core structure [*Camargo and Zebiak*, 2002]. The change in TC frequency is defined as the change in the number of genesis events in each separate basin over 10 – 20°, which corresponds to 70–80% of the tropical cyclogenesis latitudes in the GCMs, to conform with the ventilation favorability calculation. To avoid

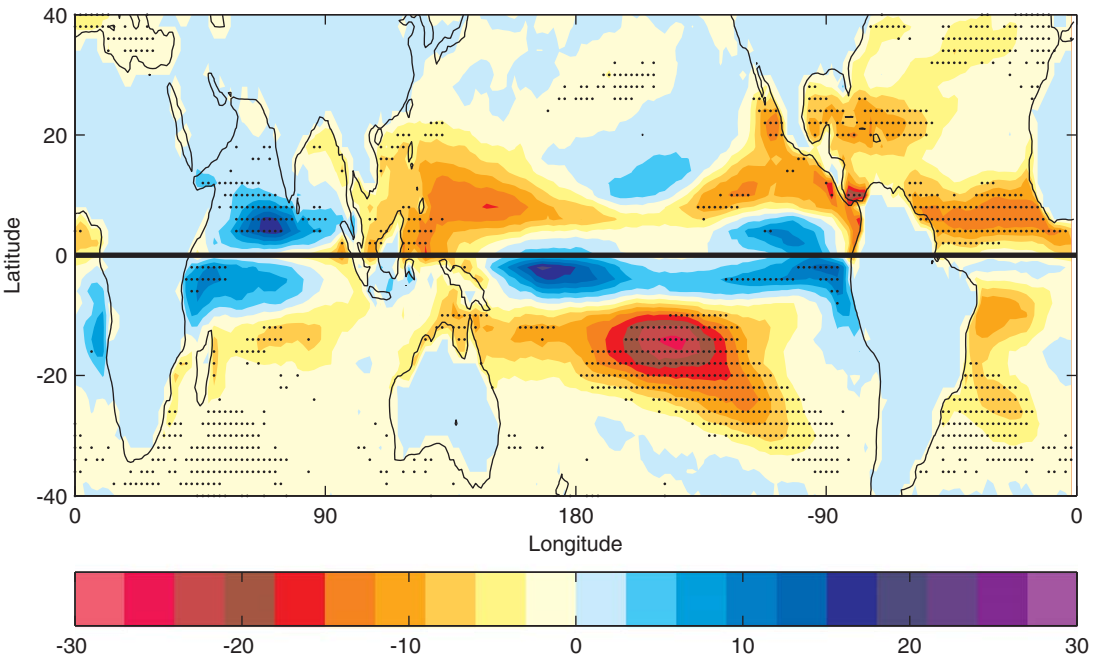

Figure 7. The eight-GCM ensemble average of the change in the ventilation favorability. Stippled areas denote where the ensemble average change exceeds the ensemble standard deviation.

small sample size leading to large outliers, a model must have at least 10 TCs in either the historical or RCP8.5 experiments in a basin in order to be included as a data point.

Figure 8 shows changes in ventilation favorability correlate well with changes in TC frequency across the basins. The rank correlation is 0.59, which is significant at the 95% level using a permutation test. The GFDL-ESM2M model in the North Atlantic (red square) and the CSIRO-Mk3.6.0 model in the Northeast Pacific (blue circle) have the largest increase in ventilation favorability and correspondingly have the largest increase in the number of TCs. The remainder of the models and basins has a decrease in ventilation favorability, implying a decrease in either the number of days or locations where the ventilation is favorable for tropical cyclogenesis. However, this does not necessarily translate to a decrease in TC frequency since the MRI-CGCM3 and GFDL-ESM2M models still indicate an increase in TC frequency in a number of basins despite a decrease in ventilation favorability. One possible explanation is that the GCMs are not sensitive enough to the interaction between ventilation and tropical disturbances due to their coarse resolution. Also, one must keep in mind that the GCMs have significant biases in TC frequency, with all underestimating TC frequency relative to current climatology

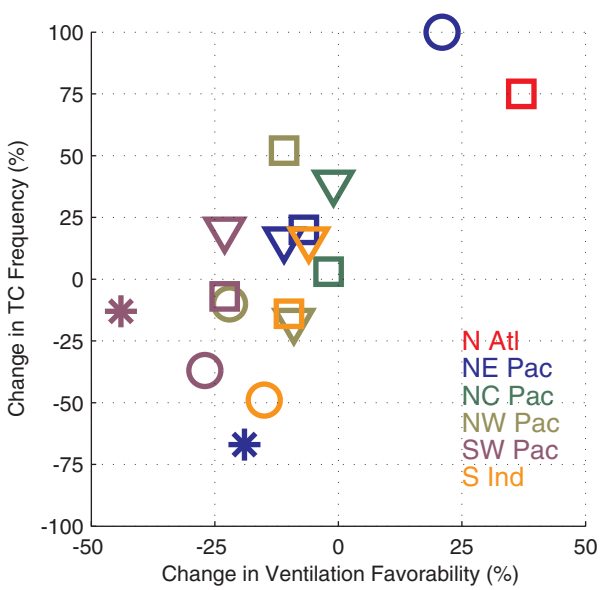

Figure 8. Change in ventilation favorability, defined as the percent change in the cumulative distribution of the daily ventilation index at the 25th percentile of the historical experiment period, versus the change in TC frequency. Data points are separated by basin, as given by the color in the legend, and model: CSIRO-Mk3.6.0 (circles), GFDL-ESM2M (squares), MIROC5 (asterisks), and MRI-CGCM3 (triangles).

[*Camargo*, 2013]. The methodology used to count the number of TCs in GCMs also yields different results. For instance, *Tory et al*. [2013] found that TC frequency decreases in the vast majority of the TC basins and GCMs, which would be more consistent with the overall decrease in ventilation favorability. The positive correlation between the changes in ventilation favorability and changes in TC frequency is what is important here, not solely the change in the latter.

Downscaling techniques to assess changes in TC frequency in the CMIP5 database give conflicting results, although the region, emissions scenario, and model suite examined in the various analyses differ [*Villarini and Vecchi*, 2012; *Emanuel*, 2013; *Knutson et al*., 2013; *Villarini and Vecchi*, 2013], making a fair comparison difficult. *Emanuel* [2013] looked at changes in global frequency and found increases in six of the CMIP5 GCMs, including MIROC5, MPI-ESMMR, MRI-CGCM3, and NCAR-CCSM4. This occurs despite the increase in the ventilation index in many of the basins (see Table 2) in these models. Ventilation is only one factor, albeit a potentially important one, among a plethora that controls genesis. There may be other positive factors affecting genesis that are outweighing the negative effects of increasing ventilation that remain to be sorted out. Moreover, this analysis only considers the environment in which tropical disturbances are embedded and not changes in the climatology of precursor disturbances themselves that may be just as important in changing TC frequency.

Next, changes in the ventilation favorability are compared with changes in TC "rapid" intensification. GCMs do not resolve the TC inner core, and hence, do not simulate the rapid intensification process with fidelity. In lieu of using the traditional definition of rapid intensification, we set the threshold for rapid intensification to be the 5th percentile of 24 h pressure falls for each GCM in the database of *Camargo* [2013] for TCs during the historical experiment period (1981–2000). The 5th percentile is motivated by observations of rapid TC intensification in the best track database for the North Atlantic [*Kaplan et al*., 2010]. The normalized rapid intensification is defined as the number of 24 h periods the threshold is exceeded in each basin divided by the basin TC count. The percent change in the normalized rapid intensification between the historical and RCP8.5 experiments is then calculated for each model and basin. For this particular analysis, the latitude band is expanded to 10 – 30° for both the normalized rapid intensification and ventilation favorability statistics to account for TCs migrating poleward after genesis. Again, a model must have at least 10 TCs in either the historical or RCP8.5 experiments in a basin in order to be included as a data point.

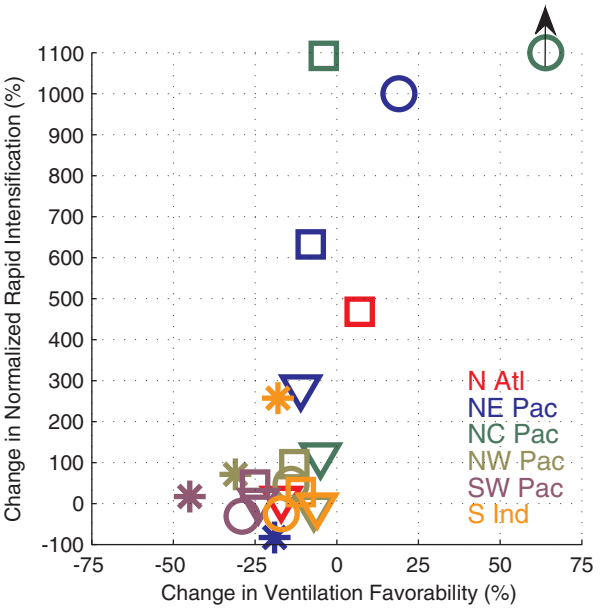

Figure 9. Similar to Figure 8, but for changes in normalized rapid intensification, defined as the number of 24 h periods with pressure falls below the fifth percentile of TCs in the historical experiment normalized by the number of TCs.

Figure 9 shows changes in the ventilation favorability correlate well with changes in the normalized rapid intensification. The rank correlation is 0.60, which is significant at the 95% level using a permutation test. Small absolute changes in the tail of the intensification distribution can lead to large relative changes, ranging from a decrease of −83% in the MIROC5 in the Northeast Pacific (blue asterisk) to an infinite increase in the CSIRO-Mk3.6.0 in the North-Central Pacific (green circle) due to there being no cases of rapid intensification in the historical experiment. A notable component of the positive correlation is the strong pick up in changes in normalized rapid intensification as changes in ventilation favorability approach zero and become positive, especially in the CSIRO-Mk3.6.0 and GFDL-ESM2M models.

The majority of the points in Figure 9 show an increase in the normalized rapid intensification, meaning each TC has a greater chance of undergoing rapid

intensification over at least one 24 h period during its lifetime in the RCP8.5 experiment compared to the historical experiment. A greater number of rapidly intensifying storms may contribute to the increase in power dissipation noted in other downscaling studies [*Emanuel*, 2013; *Villarini and Vecchi*, 2013].

The increase in normalized rapid intensification occurs despite many of the models indicating a decrease in the ventilation favorability. Again, the models could be in error due to insufficient resolution to resolve the ventilation process in TCs, or there could be some compensating effect that is canceling out the effects of ventilation. While the majority of the models do show a pronounced increase in the upper percentiles of intensification in many of the basins, there is substantial uncertainty. Such results must be interpreted with caution until it is understood what is causing these changes.

5. Conclusions

Ventilation inhibits both tropical cyclogenesis and tropical cyclone intensification. Nondimensionalizing the ventilation to form a ventilation index allows one to compare ventilation effects on TCs with changing climate in a consistent manner. The ventilation index can then be used as a proxy to infer potential changes in the statistics of tropical cyclones due to changes in ventilation.

The ventilation index is compared between 1981–2000 and 2081–2100 in eight CMIP5 models between the historical and RCP8.5 experiments. In the multimodel ensemble mean, there is an increase in the median ventilation index and a decrease in the ventilation favorability over much of the North Atlantic, near Mexico, around the Maritime Continent, and portions of the South Pacific, meaning fewer days favorable for tropical cyclogenesis or rapid intensification. The North Indian is one of the few areas that models project an increase in the ventilation favorability.

However, there is generally large regional and intermodel variability in the RCP8.5 projections of changes in the ventilation index. The large variability is due to the nonlinear nature of the ventilation index and compensation of its three components. The nondimensional entropy deficit increases significantly and the potential intensity increases slightly in all the models and across almost all TC basins, while the vertical wind shear decreases in most regions but shows more variability. All three components must be considered as a whole in this framework.

Changes in the ventilation favorability from the historical to RCP8.5 periods are significantly and positively correlated with both changes in the frequency of genesis and normalized rapid intensification. There are several caveats to this finding. First, ventilation is only one aspect that controls TCs. Due to the small sample size of TCs, it is not feasible to control for other factors, nor is it well understood what sets the climatology of TCs in individual GCMs to begin with. Second, the GCMs do not properly resolve the interaction of TCs with ventilation due to their relatively coarse resolution. Statistical-dynamical downscaling methods are an alternative to assess how ventilation controls TC statistics, but applying such a method is also dependent on how ventilation effects on TCs are handled in the downscaling itself. Third, the analysis does not apply to hybrid or baroclinic developments, which can represent a substantial portion of the total TC activity [*McTaggart-Cowan et al*., 2013].

In conclusion, there still remains large uncertainty in how the statistics of TCs will change with climate and the underlying causes behind such changes. However, there is the potential for changes in the background environment to have a significant role in controlling the distributions of both TC frequency and intensity.

Acknowledgments

The second author is supported by the National Oceanic and Atmospheric Administration Modeling Analysis and Prediction Program under grant NA11OAR4310093. We thank K. Emanuel and an anonymous reviewer for providing helpful comments. We acknowledge the World Climate Research Programme's Working Group on Coupled Modeling, which is responsible for CMIP, and we thank the climate modeling groups for producing and making available their model output. For CMIP, the U.S. Department of Energy's Program for Climate Model Diagnosis and Intercomparison provides coordinating support and led development of software infrastructure in partnership with the Global Organization for Earth System Science Portals.

References

Barnes, E. A., and L. Polvani (2013), Response of the midlatitude jets, and of their variability, to increased greenhouse gases in the CMIP5 models, *J. Clim.*, *26*, 7117–7135, doi:10.1175/JCLI-D-12–00536.1.

Bender, M. A., T. R. Knutson, R. E. Tuleya, J. J. Sirutis, G. A. Vecchi, S. T. Garner, and I. M. Held (2010), Modeled impact of anthropogenic warming on the frequency of intense Atlantic hurricanes, *Science*, *327*, 454–458, doi:10.1126/science.1180568.

Bengtsson, L., M. Botzet, and M. Esch (1996), Will greenhouse gas-induced warming over the next 50 years lead to higher frequency and greater intensity of hurricanes?, *Tellus, Ser. A*, *48*, 57–73, doi:10.1034/j.1600-0870.1996.00004.x.

Bengtsson, L., K. I. Hodges, M. Esch, N. Keenlyside, L. Kornblueh, J. Luo, and T. Yamagata (2007), How may tropical cyclones change in a warmer climate?, *Tellus, Ser. A*, *59*, 539–561, doi:10.1111/j.1600-0870.2007.00251.x.

Bister, M., and K. A. Emanuel (1997), The genesis of hurricane Guillermo: TEXMEX analyses and a modeling study, *Mon. Weather Rev.*, *125*, 2662–2682, doi:10.1175/1520-0493(1997)125⟨2662:TGOHGT⟩2.0.CO;2.

Camargo, S. J. (2013), Global and regional aspects of tropical cyclone activity in the CMIP5 models, *J. Clim.*, *26*, 9880–9902, doi:10.1175/JCLI-D-12–00549.1.

Camargo, S. J., and S. E. Zebiak (2002), Improving the detection and tracking of tropical cyclones in atmospheric general circulation models, *Weather Forecast.*, *17*, 1152–1162, doi:10.1175/1520-0434(2002)017⟨1152:ITDATO⟩2.0.CO;2.

Cram, T. A., J. Persing, M. T. Montgomery, and S. A. Braun (2007), A Lagrangian trajectory view on transport and mixing processes between the eye, eyewall, and environment using a high-resolution simulation of Hurricane Bonnie (1998), *J. Atmos. Sci.*, *64*, 1835–1856, doi:10.1175/JAS3921.1.

Dee, D. P., et al. (2011), The ERA-Interim reanalysis: Configuration and performance of the data assimilation system, *Q. J. R. Meteorol. Soc.*, *137*, 553–597, doi:10.1002/qj.828.

DeMaria, M. (1996), The effect of vertical shear on tropical cyclone intensity change, *J. Atmos. Sci.*, *53*, 2076–2088, doi:10.1175/1520-0469(1996)053⟨2076:TEOVSO⟩2.0.CO;2.

Emanuel, K. (2007), Environmental factors affecting tropical cyclone power dissipation, *J. Clim.*, *20*, 5497–5509, doi:10.1175/2007JCLI1571.1.

Emanuel, K. (2010), Tropical cyclone activity downscaled from NOAA-CIRES reanalysis, 1908–1958, *J. Adv. Model. Earth Syst.*, *2*, doi:10.3894/JAMES.2010.2.1, in press.

Emanuel, K., R. Sundararajan, and J. Williams (2008), Hurricanes and global warming: Results from downscaling IPCC AR4 simulations, *Bull. Am. Meteorol. Soc.*, *89*, 347–367, doi:10.1175/BAMS-89-3-347.

Emanuel, K. A. (1989), The finite-amplitude nature of tropical cyclogenesis, *J. Atmos. Sci.*, *46*, 3431–3456, doi:10.1175/1520-0469(1989)046⟨3431:TFANOT⟩2.0.CO;2.

Emanuel, K. A. (2013), Downscaling CMIP5 climate models shows increased tropical cyclone activity over the 21st century, *Proc. Natl. Acad. Sci. U. S. A.*, *110*, 12,219–12,224, doi:10.1073/pnas.1301293110.

Garner, S. T., I. M. Held, T. Knutson, and J. Sirutis (2009), The roles of wind shear and thermal stratification in past and projected changes of Atlantic tropical cyclone activity, *J. Clim.*, *22*, 4723–4734, doi:10.1175/2009JCLI2930.1.

Gray, W. M. (1968), Global view of the origin of tropical disturbances and storms, *Mon. Weather Rev.*, *96*, 669–700, doi:10.1175/1520-0493(1968)096⟨0669:GVOTOO⟩2.0.CO;2.

Hill, K. A., and G. M. Lackmann (2011), The impact of future climate change on TC intensity and structure: A downscaling approach, *J. Clim.*, *24*, 4644–4661, doi:10.1175/2011JCLI3761.1.

Kaplan, J., M. DeMaria, and J. A. Knaff (2010), A revised tropical cyclone rapid intensification index for the Atlantic and eastern North Pacific basins, *Weather Forecast.*, *25*, 220–241, doi:10.1175/2009WAF2222280.1.

Knutson, T. R., and R. E. Tuleya (2004), Impact of CO2-induced warming on simulated hurricane intensity and precipitation: Sensitivity to the choice of climate model and convective parameterization, *J. Clim.*, *17*, 3477–3495, doi:10.1175/1520-0442(2004)017⟨3477:IOCWOS⟩2.0.CO;2.

Knutson, T. R., J. J. Sirutis, S. T. Garner, G. A. Vecchi, and I. M. Held (2008), Simulated reduction in Atlantic hurricane frequency under twenty-first-century warming conditions, *Nat. Geosci.*, *1*, 359–364, doi:10.1038/ngeo202.

Knutson, T. R., J. L. McBride, J. Chan, K. Emanuel, G. Holland, C. Landsea, I. Held, J. P. Kossin, A. K. Srivastava, and M. Sugi (2010), Tropical cyclones and climate change, *Nat. Geosci.*, *3*, 157–163, doi:10.1038/ngeo779.

Knutson, T. R., J. J. Sirutis, G. A. Vecchi, S. Garner, M. Zhao, H. Kim, M. Bender, R. E. Tuleya, I. M. Held, and G. Villarini (2013), Dynamical downscaling projections of twenty-first-century Atlantic hurricane activity: CMIP3 and CMIP5 Model-based scenarios, *J. Clim.*, *26*, 6591–6617, doi:10.1175/JCLI-D-12–00539.1.

Marín, J. C., D. J. Raymond, and G. B. Raga (2009), Intensification of tropical cyclones in the GFS model, *Atmos. Chem. Phys.*, *9*, 1407–1417, doi:10.5194/acp-9–1407-2009.

McGauley, M. G., and D. S. Nolan (2011), Measuring environmental favorability for tropical cyclogenesis by statistical analysis of threshold parameters, *J. Clim.*, *24*, 5968–5997, doi:10.1175/2011JCLI4176.1.

McTaggart-Cowan, R., T. J. Galarneau, L. F. Bosart, R. W. Moore, and O. Martius (2013), A global climatology of baroclinically influenced tropical cyclogenesis, *Mon. Weather Rev.*, *141*, 1963–1989, doi:10.1175/MWR-D-12–00186.1.

Murakami, H., Y. Wang, H. Yoshimura, R. Mizuta, M. Sugi, E. Shindo, Y. Adachi, S. Yukimoto, M. Hosaka, S. Kusunoki, T. Ose, and A. Kitoh (2012), Future changes in tropical cyclone activity projected by the new high-resolution MRI-AGCM, *J. Clim.*, *25*, 3237–3260, doi:10.1175/JCLI-D-11–00415.1.

Nolan, D. S. (2007), What is the trigger for tropical cyclogenesis?, *Aust. Meteorol. Mag.*, *56*, 241–266.

Oouchi, K., J. Yoshimura, H. Yoshimura, R. Mizuta, S. Kusunoki, and A. Noda (2006), Tropical cyclone climatology in a global-warming climate as simulated in a 20 km-mesh global atmospheric model: Frequency and wind intensity analyses, *J. Meteorol. Soc. Jpn.*, *84*, 259–276.

Powell, M. D. (1990), Boundary layer structure and dynamics in outer hurricane rainbands. Part II: Downdraft modification and mixed layer recovery, *Mon. Weather Rev.*, *118*, 918–938, doi:10.1175/1520-0493(1990)118⟨0918:BLSADI⟩2.0.CO;2.

Rappin, E. D., D. S. Nolan, and K. A. Emanuel (2010), Thermodynamic control of tropical cyclogenesis in environments of radiative-convective equilibrium with shear, *Q. J. R. Meteorol. Soc.*, *136*, 1954–1971, doi:10.1002/qj.706.

Riemer, M., and M. T. Montgomery (2011), Simple kinematic models for the environmental interaction of tropical cyclones in vertical wind shear, *Atmos. Chem. Phys.*, *11*, 9395–9414, doi:10.5194/acp-11–9395-2011.

Riemer, M., M. T. Montgomery, and M. E. Nicholls (2010), A new paradigm for intensity modification of tropical cyclones: Thermodynamic impact of vertical wind shear on the inflow layer, *Atmos. Chem. Phys.*, *10*, 3163–3188, doi:10.5194/acp-10–3163-2010.

Simpson, R. H., and H. Riehl (1958), Mid-tropospheric ventilation as a constraint on hurricane development and maintenance, paper presented at 10th Conference on Hurricanes, Am. Meteorol. Soc., Miami Beach, Fla.

Soden, B. J., and I. M. Held (2006), An assessment of climate feedbacks in coupled ocean–atmosphere models, *J. Clim.*, *19*, 3354–3360, doi:10.1175/JCLI3799.1.

Sugi, M., H. Murakami, and J. Yoshimura (2009), A reduction in global tropical cyclone frequency due to global warming, *SOLA*, *5*, 164–167.

Tang, B., and K. Emanuel (2010), Midlevel ventilation's constraint on tropical cyclone intensity, *J. Atmos. Sci.*, *67*, 1817–1830, doi:10.1175/2010JAS3318.1.

Tang, B., and K. Emanuel (2012a), A ventilation index for tropical cyclones, *Bull. Am. Meteorol. Soc.*, *93*, 1901–1912, doi:10.1175/BAMS-D-11–00165.1.

Tang, B., and K. Emanuel (2012b), Sensitivity of tropical cyclone intensity to ventilation in an axisymmetric model, *J. Atmos. Sci.*, *69*, 2394–2413, doi:10.1175/JAS-D-11–0232.1.

Taylor, K. E., R. J. Stouffer, and G. A. Meehl (2012), An overview of CMIP5 and the experiment design, *Bull. Am. Meteorol. Soc.*, *93*, 485–498, doi:10.1175/BAMS-D-11–00094.1.

Tippett, M. K., S. J. Camargo, and A. H. Sobel (2011), A Poisson regression index for tropical cyclone genesis and the role of large-scale vorticity in genesis, *J. Clim.*, *24*, 2335–2357, doi:10.1175/2010JCLI3811.1.

Tory, K. J., S. S. Chand, J. L. McBride, H. Ye, and R. A. Dare (2013), Projected changes in late-twenty-first-century tropical cyclone frequency in 13 coupled climate models from phase 5 of the Coupled Model Intercomparison Project, *J. Clim.*, *26*, 9946–9959, doi:10.1175/JCLI-D-13-00010.1.

Vecchi, G. A., and B. J. Soden (2007a), Global warming and the weakening of the tropical circulation, *J. Clim.*, *20*, 4316–4340, doi:10.1175/JCLI4258.1.

Vecchi, G. A., and B. J. Soden (2007b), Increased tropical Atlantic wind shear in model projections of global warming, *Geophys. Res. Lett.*, *34*, L08702, doi:10.1029/2006GL028905.

Villarini, G., and G. A. Vecchi (2012), Twenty-first-century projections of north Atlantic tropical storms from CMIP5 models, *Nat. Clim. Change*, *2*, 604–607, doi:10.1038/nclimate1530.

Villarini, G., and G. A. Vecchi (2013), Projected increases in north Atlantic tropical cyclone intensity from CMIP5 models, *J. Clim.*, *26*, 3231–3240, doi:10.1175/JCLI-D-12–00441.1.

Yoshimura, J., M. Sugi, and A. Noda (2006), Influence of greenhouse warming on tropical cyclone frequency, *J. Meteorol. Soc. Jpn.*, *84*, 405–428.

Zhao, M., and I. M. Held (2010), An analysis of the effect of global warming on the intensity of Atlantic hurricanes using a GCM with statistical refinement, *J. Clim.*, *23*, 6382–6393, doi:10.1175/2010JCLI3837.1.

Zhao, M., I. M. Held, S. Lin, and G. A. Vecchi (2009), Simulations of global hurricane climatology, interannual variability, and response to global warming using a 50-km resolution GCM, *J. Clim.*, *22*, 6653–6678, doi:10.1175/2009JCLI3049.1.